Adsorption of CO2 on Hydrotalcite-Derived Mixed Oxides: Sorption Mechanisms and Consequences for Adsorption Irreversibility

ARTICLE *in* INDUSTRIAL & ENGINEERING CHEMISTRY RESEARCH · MARCH 2010

Impact Factor: 2.59 · DOI: 10.1021/ie902072a

6 AUTHORS, INCLUDING:

Marta Leon
MeadWestvaco Corporation
12 PUBLICATIONS **196** CITATIONS
SEE PROFILE

Eva Díaz
University of Oviedo
80 PUBLICATIONS **1,053** CITATIONS
SEE PROFILE

Salvador Ordóñez
University of Oviedo
165 PUBLICATIONS **2,454** CITATIONS
SEE PROFILE

Aline Auroux
Claude Bernard University Lyon 1
490 PUBLICATIONS **7,932** CITATIONS
SEE PROFILE

Adsorption of CO_2 on Hydrotalcite-Derived Mixed Oxides: Sorption Mechanisms and Consequences for Adsorption Irreversibility

Marta León,[†,‡] Eva Díaz,[†] Simona Bennici,[‡] Aurelio Vega,[†] Salvador Ordóñez,*[,†] and Aline Auroux[‡]

Department of Chemical Engineering and Environmental Technology, University of Oviedo, Julián Clavería s/n, 33006 Oviedo, Spain, and Institut de Recherches sur la Catalyse et l'Environnement de Lyon, UMR 5256, CNRS-Université Claude Bernard (UCB) Lyon 1, 2 Avenue Albert Einstein, 69626 Villeurbanne Cedex, France

Magnesium−aluminum double oxides derived from the thermal treatment of layered hydroxides (hydrotalcites) have been tested for CO_2 adsorption. The effects of various preparation parameters, such as the incorporated cation (K or Na), the mode of addition of magnesium and aluminum precursors, the presence of sonication, and the calcination temperature, on the adsorption capacity under mild conditions were studied using thermogravimetry and calorimetry. Calorimetric and FTIR data were used to explain the adsorption mechanisms leading to the undesirable irreversible adsorption. This adsorption was related to the formation of unidentate CO_2-adsorbent species with the strongest adsorption sites, whereas bidentate and surface bicarbonates lead to highly reversible adsorption. In conclusion, preparation procedures that lead to an increase in the strength of basic sites do not lead to significant increases in the adsorption capacity, but rather lead to more difficult regeneration of the saturated support.

1. Introduction

Concern about carbon dioxide emissions and their safe control and disposal has sharply increased in the past few years because of increasing awareness of climate change. Among the different sequestration techniques, gas adsorption provides key advantages, such as its low energy requirements, low costs, and ease of applicability over a relatively wide range of temperatures and pressures.[1] However, none of the adsorbents currently used in these types of processes is completely satisfactory for CO_2 abatement. Therefore, activated carbons, and especially activated carbons with increased basic character, have been proposed for carbon dioxide adsorption because of their high surface areas and pore volumes.[2] However, such materials present important limitations because of their micropore structure and low thermal stability, losing their adsorption properties at temperatures higher than 523 K. Different inorganic materials have been proposed in the literature for overcoming these limitations. Among such inorganic materials, basic zeolites (obtained by desilication or doping with electropositive ions) have been tested for this purpose.[3−7] The two main drawbacks of these materials are the high temperature sensibility of their adsorption equilibria and their poor performance in the presence of other polar gases (such as water or SO_2, often present in industrial off-gases).[3−7]

Members of a new class of inorganic materials, layered double hydroxides (LDHs), have unique properties for CO_2 adsorption. These materials, also known as hydrotalcite-like compounds, consist of stacked layers of brucite [$Mg(OH)_2$] in which some of the divalent cations (Mg^{2+}) have been substituted by trivalent cations (Al^{3+}) at the centers of octahedral sites of the hydroxide sheets whose vertexes contain hydroxide ions that are shared by three octahedral cations and point toward the interlayer region. The excess positive charge of the brucite-like layers is compensated by anions (CO_3^{2-}) in the interlayer space, where water molecules are also usually found. Reported works on hydrotalcites as CO_2 adsorbents have shown that their adsorption capacities are somewhat lower than those of other sorbents (typically lower than 1.0 mmol/g), although it depends on the constituents of the framework.[8] Likewise, the presence of water molecules has been reported to favorably influence the CO_2 adsorption of hydrotalcite-like materials.[9]

However, these materials are significantly more active for CO_2 removal after thermal decomposition,[9] being transformed into basic mixed oxides.[10,11] The basic properties of these types of materials have also been considered in the design of heterogeneous catalysts for base-catalyzed reactions, such as aldol condensations or Baeyer−Villeger reactions.[12] From these applications, the influence of different preparation variables (such as thermal decomposition temperature, nature and flow pattern of the sweep gas during thermal treatment, and presence or absence of ultrasonication treatments during preparation) on the catalytic properties has been studied. At this point, the ultrasonication of the preparation liquor has been demonstrated to have a positive effect on the surface area and catalytic activity for base-catalyzed reactions,[13] although the resulting materials have not been tested as adsorbents. In the same way, the countercation of the carbonate precursor used in the preparation (Na or K) has a significant effect on the catalytic activity for base-catalyzed reactions,[14] as some of these countercations remain in the resulting solid, providing different kinds of basic sites. Other aspects, such as the thermal decomposition method (static or under flowing gas), also have significant effects on the morphology and adsorption properties of the resulting material.

Other important points to be considered in the application of hydrotalcite-derived materials for CO_2 adsorption are the regenerability of the material (possibility of thermal regeneration of the saturated adsorbent) and the reversibility of the adsorption (possibility of desorption from the saturated adsorbent through a decrease in the adsorbate pressure). These aspects are critical for ensuring the efficient use of the adsorbent, as well as for designing industrial adsorption units (thermal desorption, pressure- and temperature-swing adsorption, etc.). Concerning regenerability, some discrepancies exist among different reported works. Some authors propose that a fraction of CO_2 is irreversibly chemisorbed on the material during the initial

* To whom correspondence should be addressed. E-mail: sordonez@uniovi.es. Tel.: +34 985 103 437. Fax: + 34 985 103 434.
[†] University of Oviedo.
[‡] CNRS-Université Claude Bernard Lyon 1.

10.1021/ie902072a
Published on Web 03/17/2010

adsorption/desorption cycles, when desorption occurs as a result of changes in the pressure at the same temperature.[15] On the other hand, regeneration of the saturated adsorbent by a thermal treatment has indicated a high reversibility for hydrotalcites.[9,16] However, all of these observations are based on gravimetric or volumetric adsorption measurements without an attempt to correlate the irreversibility of these adsorption processes with the chemical mechanism of the adsorption. At this point, infrared spectroscopy of chemisorbed species is a powerful technique for understanding adsorption mechanisms, allowing for discrimination between different adsorption sites and also providing information about the reversibility of the interaction.[17]

The present work was undertaken in an effort to fill some of the above-mentioned gaps in the literature on CO_2 adsorption on hydrotalcite-derived materials. Therefore, a systematic comparison of hydrotalcite-derived materials prepared by different methods and under different reaction conditions was made (all of them provided in the literature, but without systematic comparisons), correlating the adsorption properties with the morphological and chemical properties of the materials. In the second part of this work, the reversibility of the CO_2 adsorption in selected hydrotalcites was studied in more detail, using thermogravimetric, calorimetric, and IR-spectroscopic data to understand the different adsorption modes and their correlation with the adsorption reversibility.

2. Experimental Section

2.1. Synthesis of Mixed Oxides. Mg−Al LDHs with a Mg/Al ratio of 3 were synthesized by coprecipitation under conditions of low and high supersaturation. Both methods have been described in the literature for the preparation of this type of material.[18] In general, it is accepted that low supersaturation usually leads to precipitates with higher crystallinity than those obtained under high supersaturation, because under the former conditions, the rate of crystal growth tends to be higher than the rate of nucleation.[18]

For coprecipitation at low supersaturation (constant pH), 1 M solutions of $Mg(NO_3)_2 \cdot 6H_2O$ (Fluka, >99%) and $Al(NO_3)_3 \cdot 9H_2O$ (Panreac, 98%) were mixed in a 3:1 molar ratio. A volume of 150 mL of this solution was added dropwise to 100 mL of 0.2 M K_2CO_3 (Panreac, 99%) under vigorous stirring at 333 K. The pH was kept at 10 through addition og appropriate quantities of 1.6 M NaOH (Prolabo, 98%) solution. For coprecipitation at high supersaturation (variable pH), 150 mL of the same 3:1 mixed Mg and Al solution was added to 200 mL of a base solution containing 1.6 M NaOH and 0.1 M Na_2CO_3 (Probus, 98%) under stirring. An analogous synthesis was carried out using K_2CO_3 instead of Na_2CO_3 to study the possible influence of the cation.

In all cases, the mixture was aged at 353 K for 24 h before centrifugation. The influence of ultrasound irradiation of the mixture was taken into account by preparing a new series of materials following both precipitations at low and high supersaturation under sonication. This procedure was carried out at room temperature, and the gels obtained were not aged.

The precipitate was then separated by high-speed centrifugation, washed in deionized water to remove the alkali metals and nitrate ions until pH 7 was reached, and dried in oven at 373 K for 24 h. The resulting hydrotalcites were calcined at 723 or 973 K for 7 h to obtain the mixed oxides. This heat treatment was applied in two different ways, namely, in a furnace or under an air flow, with the temperature raised at 5 K/min in both cases.

The samples are labeled using a number "1" or "2" depending on whether they were synthesized at low or high supersaturation, respectively, followed by "K" or "Na" in reference to the carbonate counteranion. In the case of samples prepared under sonication, "US" is added. For the calcined samples, the calcination temperature is included in kelvin ("723" or "973"), and finally, "M" or "F" indicates whether the calcination was carried out in a furnace or under flowing air, respectively.

2.2. Materials Characterization. Chemical analysis of Mg, Al, Na, and K in the synthesized samples was performed using an HP 7500c inductively coupled plasma mass spectrometer. The samples were dissolved in 1% HNO_3 (1:250), and Rh was used as the internal standard.

The textural properties of the samples were determined by N_2 adsorption−desorption isotherms at 77 K on a Micromeritics ASAP 2000 instrument. Prior to the analysis, the samples were outgassed in a vacuum ($<10^{-3}$ kPa) at 403 K for 6 h. Separate thermogravimetry−mass spectrometry (TG−MS) analyses of samples outgassed under these conditions indicated the total removal of adsorbed water using this procedure. The surface areas (S_{BET}) and average pore diameters (D_p) were calculated according to the Brunauer−Emmett−Teller (BET) method, whereas the pore size distributions and total pore volumes (V_p), corresponding to the cumulative pore volumes between 170 and 30000 nm, were determined from the desorption branch using the Barrett−Joyner−Halenda (BJH) method. Finally, the micropore volumes (V_{micro}) were obtained using the Harkins and Jura t method.

The formation of the basic mixed oxides from the synthesized hydrotalcites was characterized by thermogravimetric analysis in a thermogravimetry−differential scanning calorimetry (TG−DSC) instrument (Setaram, Sensys). For this purpose, a sample of hydrotalcite (10 mg) and α-alumina as an inert reference material were heated in Pt crucibles at a heating rate of 5 K/min from 298 to 1073 K under a N_2 atmosphere at a flow rate of 20 mL/min. Temperature-programmed desorption (TPD) experiments were carried out in a Micromeritics TPD/TPR 2900 apparatus connected to an MS detector (Pfeiffer Vacuum-300). Samples were treated in an analogous way as in the thermogravimetric analysis with the aim of analyzing the decomposition gases.

The crystalline structure of the hydrotalcites and the derived mixed oxides was studied by X-ray diffraction (XRD) using a Philips X'Pert Pro powder diffractometer equipped with a Cu Kα radiation source (0.15418 nm) and operating in a 2θ range of 5−85° at a scanning rate of 0.02°/s. The X-ray tube voltage and current were set at 45 kV and 40 mA, respectively.

2.3. CO_2 Adsorption. Thermogravimetric adsorption of CO_2 (Praxair, >99.99%) on mixed oxide was measured using the above-mentioned TG−DSC instrument. Samples were pretreated in situ at 723 or 973 K in pure N_2 flowing at 20 mL/min before measurement of the CO_2 adsorption at 0.1 MPa and temperatures of 323 and 373 K. A constant flow of 20 mL/min was maintained during the CO_2 sorption experiments for 10 h, followed by desorption under a N_2 flow and thermal conditions (723 or 973 K, at 5 K/min). Finally, the sample was cooled to the initial adsorption temperature, and a second cycle was started. Similar experiments were carried out at a pressure of 6.7 kPa of CO_2 instead of at atmospheric pressure using a CO_2/He gas mixture. This experimental approach has been widely used in the literature for adsorption studies.[9,19]

Calorimetric experiments were carried out in a Tian-Calvet microcalorimeter (C80, Setaram) linked to a volumetric line. The adsorption was executed by repeatedly sending small doses

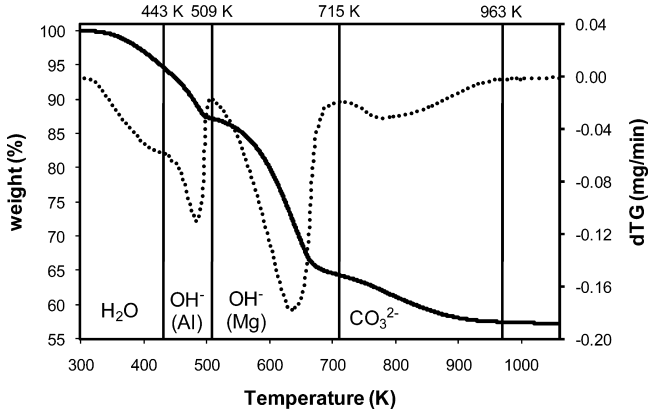

Figure 1. Thermogram for the formation of the mixed oxide from the 1K hydrotalcite precursor.

of gas onto the initially outgassed solid until a final equilibrium pressure of 6.7 kPa was reached. Before adsorption, about 80 mg of mixed oxide was outgassed overnight at 623 K under a vacuum (10^{-6} kPa). The equilibrium pressure was measured after each dose with a Barocel capacitance manometer (Datametrics). The adsorption temperature was maintained at a constant value. Once the first adsorption cycle had completed, the system was evacuated to a pressure of 10^{-7} kPa to remove the physisorbed CO_2, and a second adsorption cycle was performed. The difference between the primary and secondary isotherms is the irreversibly chemisorbed amount (V_{irr}).

To gain further understanding on the adsorption mechanisms, the chemical structure of the chemisorbed CO_2 was characterized by Fourier transform infrared (FTIR) spectroscopy. Data were obtained using a Bruker Vector 22 FTIR spectrophotometer [deuterated triglycine sulfate (DTGS) detector], in the 4000−400 cm^{-1} range, with a resolution of 2 cm^{-1} and using 100 scans. An inverted T-shaped Pyrex cell containing the sample pellet was used. The two ends of the short arm of the T were fitted with CaF_2 windows. The self-supporting wafer (20 mg, 18-mm diameter) was first activated in situ at 573 K in flowing oxygen overnight, then evacuated at the same temperature for 2 h, and finally exposed to CO_2 (1 kPa) at room temperature for 5 min. Spectra were recorded at room temperature after CO_2 adsorption and subsequent evacuation for 20 min at room temperature, 323, 373, 423, 473, 573, and 673 K. The background spectrum was measured before adsorption and used to correct the other spectra by absorbance subtraction.

3. Results and Discussion

3.1. Materials Characterization. 3.1.1. Study of the Thermal Degradation of the Hydrotalcite Precursors. The thermal evolution of the hydrotalcite structure into the mixed oxides is a key point because the resultant oxides are used for CO_2 adsorption in this study. The typical thermogravimetric−differential thermogravimetric (TG−DTG) profile of the hydrotalcite decomposition is shown in Figure 1. All of the prepared Mg−Al−CO_3 samples showed four decomposition steps leading to the corresponding mixed oxides. A first region showed water (mass 18) loss without associated peaks in the DSC curve. Most of the loosely held water in the interlayer space was lost before the materials reached 463 K. The second (443−530 K) and third (510−743 K) stages showed intense endothermic peaks. These peaks correspond to the loss of the OH^- groups bonded to Al^{3+} and to Mg^{2+}, respectively.[20,21] Finally, decarbonation is observed between 700 and 970 K.[20,21] There are no marked differences among the studied hydrotalcite precursors, in either the peak temperatures or the weight loss, which is consistent with the literature in both cases.[9,22] However, it was observed that the ultrasonication and the mixing of the reactants at low supersaturation led to higher incorporation of carbonates in the hydrotalcite structure.

Table 1. Molar Ratios of the Metal Constituents of the Hydrotalcite-Derived Materials and Crystallite Sizes of the Resulting Materials

sample	Mg/Al	Na/Al	K/Al	K/Na	L_{200} (nm)
1K	3.0	0.20	0.05	0.24	
1K723F	2.9	0.26	0.03	0.11	5.1
1K723M	3.0	0.20	0.02	0.09	4.2
1K973F	2.9	0.26	0.02	0.08	5.5
1K973M	3.0	0.19	0.03	0.15	5.5
2K	3.0	0.06	0.01	0.23	
2K723F	2.9	0.13	0.01	0.07	4.4
2K723M	2.9	0.09	0.01	0.13	4.7
2K973F	2.9	0.09	0.01	0.07	5.2
2K973M	2.9	0.10	0.02	0.15	5.4
1KUS	3.0	0.46	0.03	0.07	
1KUS723F	3.0	0.25	0.02	0.07	4.1
1KUS973F	3.0	0.28	0.02	0.08	5.2
2KUS	3.0	0.11	0.01	0.07	
2KUS723F	3.0	0.11	0.01	0.05	4.4
2KUS723M	3.0	0.07	0.00	0.04	4.4
2KUS973F	3.0	0.07	0.00	0.02	5.2
2Na	2.9	0.12	0.00	0.00	
2Na723M	2.9	0.12	0.00	0.02	4.7
2Na973M	2.9	0.13	0.00	0.02	5.4

Hence, two temperatures were chosen in this work for the decomposition of the hydrotalcites. Mixed oxides obtained upon treatment at 723 K should be in a completely dehydroxylated state, whereas the samples treated at 973 K should have even overcome the decarbonation stage to become an amorphous metastable, mixed solid solution.[21] As mentioned before, the behavior observed during the calcinations is very similar to that reported in the literature. However, very different decomposition temperatures were chosen in the works reported in the literature, namely, 673,[23] 723,[13] 823,[19,20] and 973[23] K, without a systematic comparison between the resulting materials.

3.1.2. Elemental Analysis. The elemental composition of the hydrotalcites and mixed oxides synthesized is summarized in Table 1. The Mg/Al ratio matches with the theoretical value, corresponding to the Mg/Al ratio in the cation solution. Small amounts of Na and K could be detected, which might have come from some reagents trapped during the crystallization process.

3.1.3. Crystallographic Characterization. X-ray diffraction patterns of the raw materials (Figure 2) showed the typical diffractograms of hydrotalcite-like materials (JCPDS 14-191). The sharp and intense peaks at $2\theta \approx 11°$, 23°, and 34° correspond to the (003), (006), and (009) planes, indicating a well-formed crystalline layered structure with a rhombohedral symmetry (3R). Assuming a 3R stacking sequence, an interlayer spacing, c, of around 2.34 nm and an average metal−metal distance, a, of 0.305 nm were obtained, both similar to the theoretical values for brucite layers.[24] In some of the diffractograms, $NaNO_3$ (JCPDS 36-1474) trapped in the hydrotalcite structure during the synthesis process was also detected.[25]

Regarding the mixed oxides, the XRD patterns reveal that the layered structure was completely collapsed after heat treatment. Only weak, broad peaks reflections at ∼37°, 43°, and 62° were observed, which correspond to diffraction by the (111), (200), and (220) planes of periclase (MgO, JCPDS 45-946). The aluminum compounds should be well-dispersed or should form an amorphous phase.[26] The crystallite size of the mixed oxides was calculated from the plane (200) using the Debye−Scherrer equation;[27] values are included in Table 1.

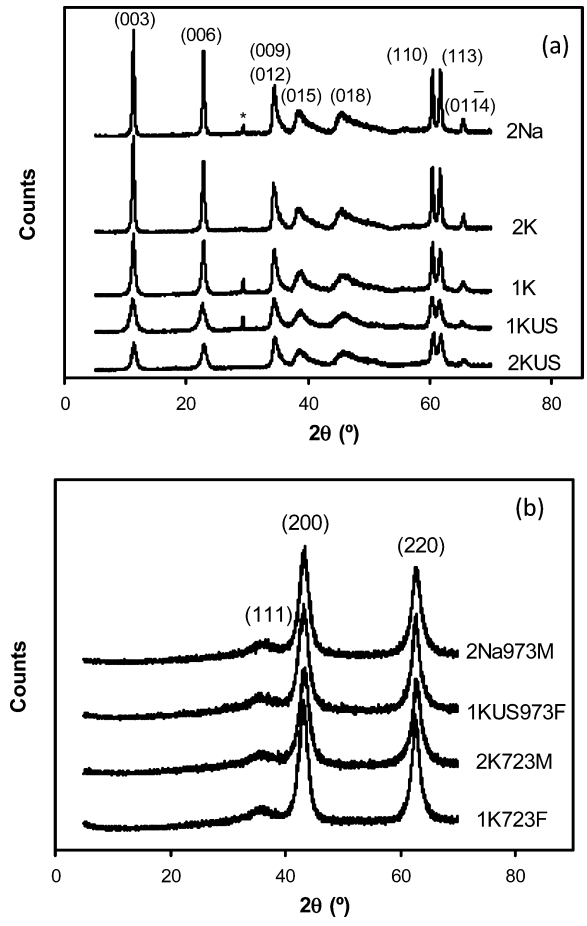

Figure 2. XRD patterns of the (a) as-prepared hydrotalcites and (b) several mixed oxides obtained by different methods.

Whereas, for the hydrotalcite samples, crystallinity increases with coprecipitation for the high-supersaturation method and for use of Na_2CO_3 instead of K_2CO_3, no clear trends were found for the mixed oxides. The precursor seems to have only a limited effect on the crystallinity of the mixed oxides, with the calcination temperature being the main parameter affecting crystallinity. Therefore, the highest crystallinities were observed for the oxides calcined at 973 K, in good agreement with the literature findings,[22,23] whereas no significant differences were observed between the heat treatment in a furnace or in flowing air. The sonication treatment was found to generally lead to slightly lower crystallinities, as a result of acoustic cavitation effects, which cause particle fragmentation.[13] This effect is more marked for the hydrotalcites prepared using the high-supersaturation method, which is in good agreement with the higher relative ion concentrations in comparison with the other method.

3.1.4. Morphological Characterization. The surface areas and pore volumes of the materials were determined by nitrogen adsorption−desorption isotherms at 77 K of both hydrotalcites and mixed oxides (Figure 3). All of the materials characterized clearly corresponded to type IV (mesoporous solids), according to the IUPAC classification. Analysis of the hysteresis loops indicates that samples synthesized by the low-supersaturation method, either under sonication or not (Figure 3, parts c and a, respectively), did not exhibit any limiting adsorption at high relative pressure, which is characteristic of type H3 hysteresis loops, corresponding to aggregates of platelike particles giving rise to slit-shaped pores. On the other hand, samples synthesized by the high-supersaturation method in the absence of ultrasound irradiation (Figure 3, parts b and e) present hysteresis loops more similar to type H1, which is often associated with porous materials consisting of agglomerates or compacts of approximately uniform spheres in a fairly regular array and, hence, having narrow distributions of pore size. Finally, the family of samples prepared by the high-supersaturation method under sonication could be correlated with type H2 loops, corresponding to a complex and interconnected pore structure. In general, the porous structure patterns were maintained after the thermal decomposition, despite the observed increases in surface area.

The textural properties of the samples are summarized in Table 2. As expected, heat treatment of the samples enhanced their specific surface areas and mesopores volumes, especially at 973 K under air flow. With regard to the average pore diameters, the trend is not as clear, varying between 9.3 and 30.4 nm. In any case, these values ensure that the pore diffusion is not limiting with respect to the subsequent CO_2 adsorption studies.[28] According to Figure 1, at both treatment temperatures, the anions in the interlayer are decomposed, and the material is completely dehydroxylated, obtaining a three-dimensional structure constituted by a regular oxygen cubic close-packed network with a cation distribution in the interstices. The strains associated with the formation of this three-dimensional structure and with the compression−expansion of the octahedral layer are related to a significant increase in surface area.[10] The contribution of the microporosity to the total volume is very small (around 1%).

Mixed oxides prepared under low-supersaturation conditions showed higher pore sizes and pore volumes. In this way, hydrotalcites synthesized by this method display type H3 hysteresis, which is usually associated with the presence of open large pores.[29] Concerning sonication, no relevant increase in either surface area or pore volume was detected by this method, although lower crystallite sizes were obtained in mixed oxides derived from sonicated samples. In agreement with the XRD results, the samples prepared using K_2CO_3 showed higher specific surface areas. Pore volume was also higher, although pore size was lower and no significant differences were observed for micropore volume.

3.2. Characterization of the CO_2 Adsorption over the Mixed Oxides. 3.2.1. Screening of the Different Prepared Mixed Oxides for CO_2 Adsorption. Figure 4 shows the adsorption of carbon dioxide in pure/single CO_2 gas system on the different mixed oxides tested. After a rapid initial uptake of CO_2 at low pressures, all of the samples exhibited a region of slow adsorption kinetics. This slow kinetics was already reported in the literature for this type of material.[30,31] No significant differences between different materials studied in this work were observed. The adsorption study was conducted at 323 and 373 K and 0.1 MPa. A decrease in the uptake as the adsorption temperature increased from 323 to 373 K was observed (Table 3), as expected for an exothermic adsorption process. The differences in adsorption capacity can be caused by differences in both surface area and surface chemistry. Comparison of the values of the adsorption capacities in millimoles per gram and micromoles per square meter shows that, in the case of the hydrotalcite-like materials prepared with sodium carbonate, the lower performance is mainly caused by their lower surface area. However, in the case of the sonicated samples, their better performance is not correlated with increases in the surface area, suggesting chemical changes on the material surface. The effects of the preparation procedure, temperature, and environment of the calcinations are extremely complex to evaluate, as they are interrelated. All of these facts suggest that

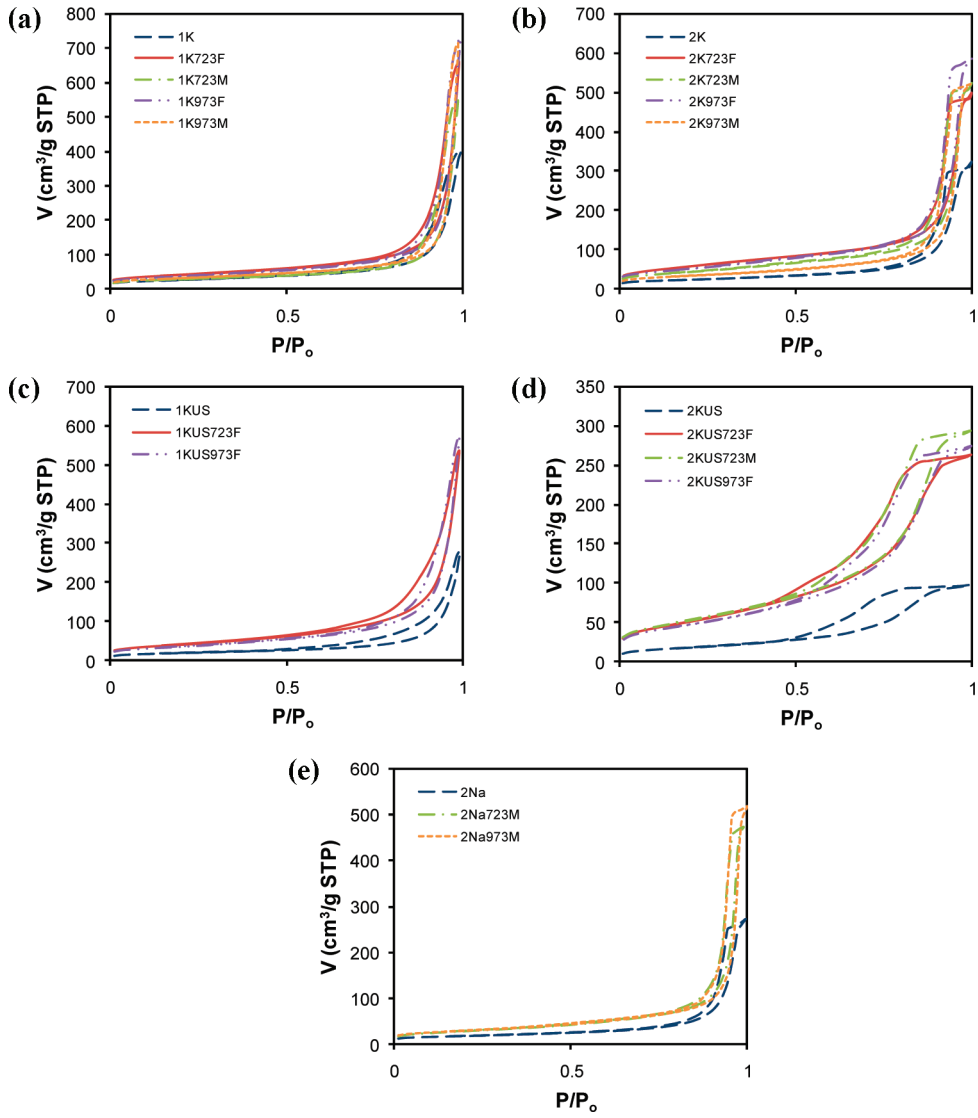

Figure 3. N_2 adsorption−desorption isotherms at 77 K for the hydrotalcite precursors and the resulting mixed oxides.

Table 2. Textural Properties of LDHs and Mixed Oxides

sample	S_{BET} (m^2/g)	D_p (nm)	V_p (cm^3/g)	V_{micro} (cm^3/g)
1K	86	24.4	0.611	0.006
1K723F	137	24.9	1.007	0.011
1K723M	94	30.4	0.865	0.008
1K973F	131	26.6	1.113	0.011
1K973M	116	29.3	1.103	0.012
2K	82	23.3	0.477	0.009
2K723F	190	15.8	0.757	–
2K723M	151	20.8	0.793	0.006
2K973F	172	20.7	0.888	0.003
2K973M	114	27.7	0.797	0.008
1KUS	64	22.9	0.420	0.005
1KUS723F	142	19.3	0.816	0.009
1KUS973F	124	23.4	0.870	0.010
2KUS	65	9.3	0.151	0.001
2KUS723F	174	9.3	0.410	–
2KUS723M	180	10.1	0.457	0.002
2KUS973F	159	10.5	0.424	0.002
2Na	62	26.5	0.410	0.009
2Na723M	100	27.6	0.728	0.005
2Na973M	102	28.9	0.790	0.009

the adsorption of CO_2 on these materials combines physisorption and chemisorption effects, as discussed more fully in subsequent sections.

To perform a systematic study of the process parameters, the family of the materials calcined at 723 K under flowing gas and those prepared using K as the carbonate countercation were used for further studies. This family of materials presents the highest average adsorption capacities, and their preparation is easy and reproducible.

3.2.2. Detailed Adsorption Studies Combining Thermogravimetry and Calorimetry. As stressed in the Introduction, not only the adsorption capacity is important in the selection of a given adsorbent, but also the reversibility of the adsorption. To gain further understanding of the reversibility of this interaction, different adsorption−desorption cycles were carried out in the TG instrument. To perform these studies at the same conditions as the calorimetric experiments, the TG experiments were also carried out at lower CO_2 pressures (6.7 kPa, working with CO_2−He mixtures). In both cases, regeneration was measured by heating the sample after CO_2 adsorption from the adsorption temperature (323 K) to 723 at 5 K/min under a N_2 flow. After this, a second adsorption cycle was recorded.

The results are summarized in Table 4. Regenerability (R) is expressed as the percentage ratio between the adsorption capacities in the second and first cycles. At both adsorption pressures, it was observed that the regenerability of the mixed oxides synthesized by coprecipitation at low supersaturation was improved compared to those prepared by the other method. Thus, this coprecipitation method showed an increased capacity

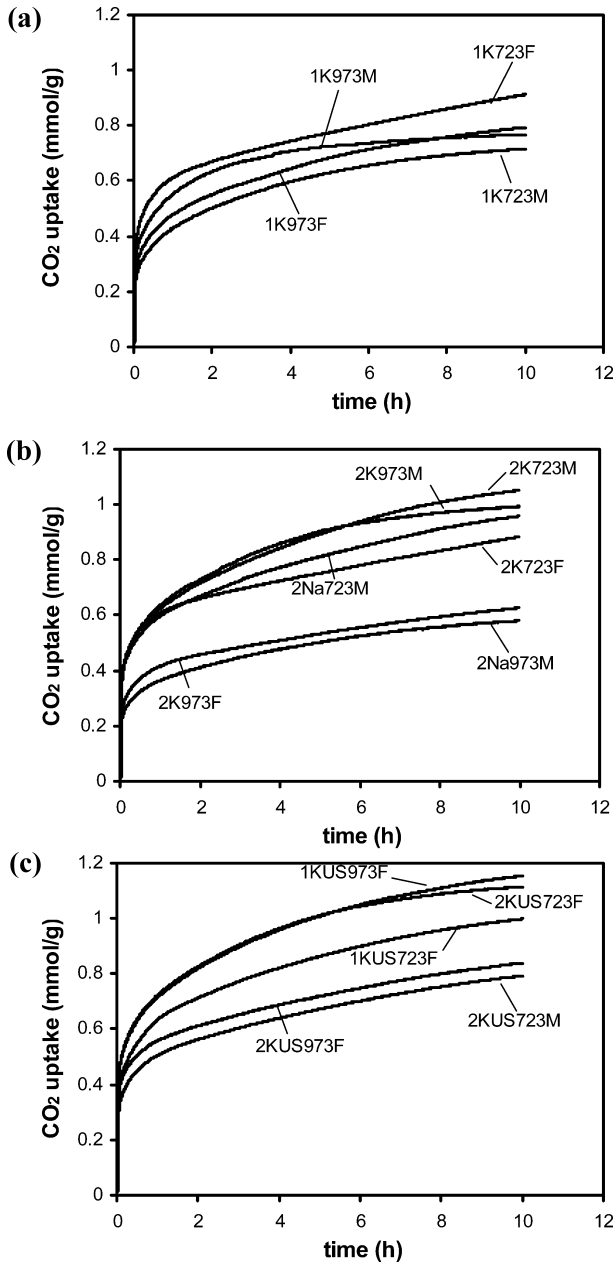

Figure 4. CO_2 uptake over the mixed oxides under study at 323 K and 0.1 MPa, measured by thermogravimetry.

of adsorption and regenerability, although the surface area and pore volume were lower than for the other method. Concerning the effect of temperature, it was observed that the regenerability of the adsorption increased as the temperature decreased—at least for nonsonicated samples—suggesting that the irreversibility was mainly caused by chemical reactions of the CO_2 with the basic sites of the adsorbent. Comparison of the experiments performed at both pressures indicates that the reversibility increased at lower pressures, which suggests that the local concentration of the adsorbate plays a key role in the formation of the irreversibly adsorbed compound.

As commented before, equilibrium adsorption isotherms at 6.7 kPa and 323 K of these mixed oxides were also recorded by microcalorimetry (Figure 5). The shape of these curves suggests the presence of combined chemisorption and physisorption (even multilayered). Therefore, a Langmuir transformation fit of the curves was found to provide good results at low coverages but not to fit the data at higher converages, suggesting multilayer adsorption.

Table 3. CO_2 Adsorption Capacities, Expressed as mmol/g and μmol/m^2, at Atmospheric Pressure for the Different Mixed Oxides Studied in This Work[a]

	mmol/g		μmol/m^2	
sample	323 K	373 K	323 K	373 K
1K723F	0.90	0.72	6.59	5.25
2K723F	0.87	0.67	4.59	3.53
1KUS723F	0.99	0.84	7.00	5.94
2KUS723F	1.11	0.72	6.37	4.14
1K723M	0.71	0.61	7.59	6.49
2K723M	1.04	0.61	6.88	4.03
2KUS723M	0.79	0.57	4.39	3.16
2Na723M	0.96	0.50	9.56	5.00
1K973F	0.78	0.78	5.98	5.96
2K973F	0.62	0.58	3.61	3.37
1KUS973F	1.15	0.83	9.28	6.69
2KUS973F	0.83	0.54	5.21	3.39
1K973M	0.77	0.45	6.59	3.88
2K973M	0.98	0.61	8.56	5.33
2Na973M	0.58	0.40	5.69	3.92

[a] Adsorption capacities were determined by TG at 0.1 MPa and 323−373 K.

The combined physisorption and chemisorption isotherm was first determined, and the sample was then evacuated to remove only the reversibly adsorbed CO_2. The adsorption isotherm was then obtained again, yielding the reversibility of the adsorption. The irreversible adsorption was determined by the difference between the isotherms of the first and second adsorption cycles at the operating pressure. The results are summarized in Table 4.

In general, it is observed that the materials prepared in the presence of sonication presented both lower adsorption capacities and higher adsorption irreversibility. At first appearance, this first observation contradicts the highest adsorption capacity found for these materials at 0.1 MPa reported in Table 3. However this differential behavior can be understood by considering that, at 0.1 MPa, the contribution of physisorption is more important, as physisorption is mainly controlled by the external surface area, which is, in general terms, higher for the sonicated samples. Regarding the differences between the samples prepared at low and high supersaturation, there is a good agreement between the experiments carried out at low and high pressure. In both cases, the materials prepared by the low-supersaturation method presented the highest adsorption capacities and reversibilities.

Adsorption microcalorimetry is a powerful technique for the characterization of basic properties of solids because it gives the concentration of sites and their distribution.[32] The heat of adsorption of CO_2 can be taken as a measurement of the basic strength of the adsorption sites, and therefore, the distribution of basic sites can be obtained using the differential heat of adsorption as a function of coverage (Figure 6). The increase in the CO_2 uptake is accompanied by a continuous decrease in the differential heat from initial values between 95 and 160 kJ/mol to low values (<25 kJ/mol), which indicates a heterogeneity of the strength of the basic sites. The limit of weak interaction, which can be reasonably attributed to physical adsorption and thus neglected in calculating the concentration of basic sites, is 25 kJ/mol for CO_2 adsorption.[33] The strongest sites can be separated into three groups according to their strength: strong (Q > 150 kJ/mol), medium (120 < Q < 150 kJ/mol) and weak (Q < 90 kJ/mol).[29,34] Figure 6 also shows the distribution of the strength of the basic sites, where no strong sites were presented by the samples. The absence of these sites is positive from the point of view of the application of these materials as adsorbents, because these sites lead to surface carbonates

Table 4. Regenerability, Total CO_2 Adsorption Capacity, and Irreversible and Reversible Components

sample	$R_{100\ kPa,323\ K}$[a] (%)	$R_{100\ kPa,373\ K}$[a] (%)	$R_{6.7\ kPa,323\ K}$[a] (%)	V_{tot}[b] (mmol/g)	V_{irr}[c] (mmol/g)	V_{rev}[d] (%)
1K723F	83	78	95	1.020	0.142	86.1
1KUS723F	76	79	91	0.479	0.160	66.6
2K723F	80	80	90	0.806	0.143	82.2
2KUS723F	73	78	87	0.569	0.189	66.7

[a] Regenerability, from thermogravimetric measurements. [b] Total amount of CO_2 adsorbed as determined by microcalorimetry. [c] Irreversibly adsorbed CO_2 (microcalorimetry). [d] Percentage of the reversible contribution to the total capacity (microcalorimetry).

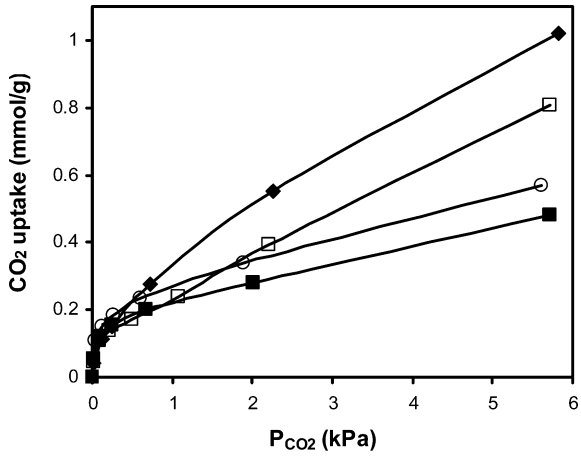

Figure 5. CO_2 adsorption isotherms at 323 K and 6.7 kPa, measured by microcalorimetry for (◆) 1K723F, (□) 2K723F, (■) 1KUS723F, and (○) 2KUS723F.

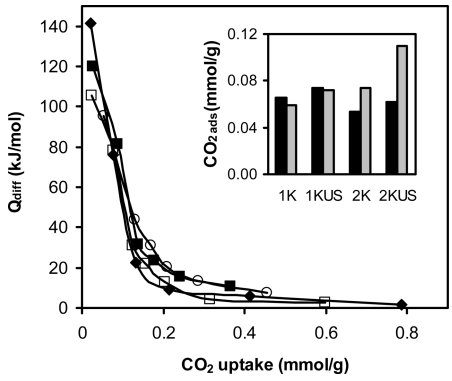

Figure 6. Differential heats of CO_2 adsorption vs coverage at 323 K on (◆) 1K723F, (□) 2K723F, (■) 1KUS723F, and (○) 2KUS723F. Distribution of interaction strengths of carbon dioxide adsorption on the mixed oxides: black, $150 > Q > 90$ kJ/mol; gray, $90 > Q > 30$ kJ/mol.

(irreversible adsorption). The sum of the weak and medium adsorption sites is higher for the ultrasonicated samples, suggesting that these adsorption sites are also responsible for irreversible adsorption phenomena. Comparing the two supersaturation procedures, it is observed that the low-supersaturation method led to the highest concentration of the medium-strength sites, whereas the other procedure showed the opposite trends.

3.2.3. Spectroscopic Characterization of the Adsorbed Species (FTIR Spectroscopy). To further characterize the basic sites of the mixed oxides, infrared spectroscopic studies of the surfaces of the mixed oxides after CO_2 adsorption and desorption at temperatures up to 673 K were determined. Analysis of the spectra provides useful information on the nature of the species formed upon CO_2 adsorption, complementing the conclusions drawn from microcalorimetry about the strengths and relative amounts of basic sites.

Figure 7 presents FTIR spectra in the 900−1900 cm^{-1} range of the previously selected mixed oxides after CO_2 adsorption at room temperature and subsequent desorption under a vacuum

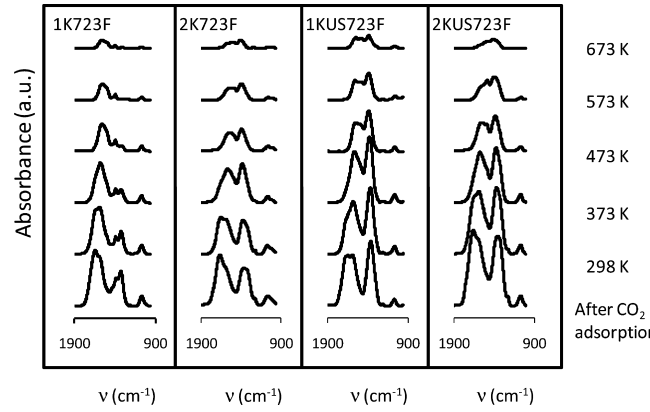

Figure 7. IR spectra of CO_2 adsorbed on mixed oxides after samples had been degassed at different temperatures: 323, 373, 423, 473, 573, and 673 K.

Scheme 1. Species Formed upon CO_2 Adsorption

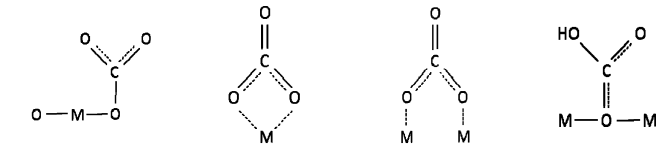

at temperatures up to 673 K. The formation of the different species stems from the presence of sites with different basic strengths: bicarbonates require surface hydroxyl groups (OH, weak base sites), whereas carbonates are formed on surface oxygen atoms of different coordination degree, leading to unidentate and bidentate, chelating or bridging, carbonates. Unidentate species are formed on oxygen ions showing the lowest coordination number (O^{2-}, strong base sites), whereas chelating and bridging bidentate carbonates require the participation of an adjacent cationic site ($M^{n+}-O^{2-}$ pairs, medium-strength base sites)[35] (Scheme 1).

Computer decomposition of the spectra and evaluation of the resistance to evacuation and the spectral parameter $\Delta\nu_3$ were used for the assignation of the species modes. $\Delta\nu_3$ represents the splitting of the degenerate asymmetric ν_{CO} vibration, ν_3 mode (at 1415 cm^{-1} for the free carbonate ion in inorganic salts), due to the lower D_{3h} symmetry of the carbonate ion when it is adsorbed. In the adsorbed state, the symmetry is lowered, and the species formed generally present two ν_{CO} bands on either side of the wavenumber 1415 cm^{-1} whose splitting depends on the nature of the carbonate.[36] The splitting, $\Delta\nu_3$, can be considered as a measure of the strength of the base sites: the lower the splitting, the stronger the basic site.[36] $\Delta\nu_3$ values of about 100, 300, and 400 cm^{-1} are generally ascribed to unidentate, chelating bidentate, and bridging bidentate structures, respectively.[37]

Table 5 summarizes the assigned bands for each species in the four samples after CO_2 adsorption at room temperature; the area of the decomposed peaks corresponding to each species,

Table 5. Bands of Species Formed upon CO_2 Adsorption on Mixed Oxides[a]

sample	bb	h	cb	u	u	u	u	bb/cb	h	u/bb/cb
1K723F			**1650**	**1575**	**1505**	**1435**	**1385**	**1325**		**1065**
			(55)	(12)	(10)	(6)	(9)	(18)		(4)
			[325]	[190]	[70]					
1KUS723F	**1730**	**1685**	**1645**	**1590**	**1530**	**1410**	**1360**	**1305**	**1215**	**1070**
	(7)	(19)	(13)	(26)	(18)	(10)	(39)	(5)	(0.3)	(2)
	[425]		[340]	[230]	[120]					
2K723F	**1740**	**1690**	**1655**	**1590**	**1525**	**1400**	**1355**	**1300**	**1225**	**1050**
	(5)	(14)	(19)	(17)	(10)	(6)	(28)	(5)	(1)	(6)
	[440]		[355]	[235]	[125]					
2KUS723F	**1755**	**1690**	**1650**	**1590**	**1500**	**1385**	**1355**	**1310**	**1220**	**1070**
	(3)	(36)	(14)	(52)	(22)	(16)	(43)	(18)	(2)	(3)
	[445]		[340]	[235]	[115]					

[a] In bold, infrared bands (cm^{-1}) after CO_2 adsorption at room temperature; in parentheses, areas of the decomposed peaks; in square brackets, $\Delta\nu_3$ values (cm^{-1}).

which is proportional to the concentration of each type of basic site present in the samples; and the $\Delta\nu_3$ values. The different species have been labeled as u (unidentate carbonates), cb (chelating bidentate carbonates), bb (bridged bidentate carbonates), and h (bicarbonates). It should be noted that all of the previously mentioned species were present in samples 1KUS723F, 2K723F, and 2KUS723F, whereas no appreciable bands of bicarbonates or bridged bidentate carbonates were detected in the 1K723F sample. Bands at around 1690 and 1220 cm^{-1} can be assigned to the asymmetric O−C−O stretching vibration (asym ν_{O-C-O}) and C−OH bending (δ_{COH}) modes, respectively, of bicarbonate. Pairs of bands at 1575−1590 cm^{-1} (asym ν_{O-C-O})/1355−1385 cm^{-1} (sym ν_{O-C-O}) and 1500−1530 cm^{-1} (asym ν_{O-C-O})/1385−1435 cm^{-1} (sym ν_{O-C-O}), with $\Delta\nu_3$ in the ranges 190−235 and 70−125 cm^{-1}, respectively, might correspond to two different unidentate structures. The first value of $\Delta\nu_3$ is higher than the above-reported value for unidentate species; nevertheless, the similar thermal stabilities displayed by the two pairs of bands suggest that they could originate from analogous species. Bands at 1645−1655 and 1730−1755 cm^{-1} could belong to the asymmetric ν_{O-C-O} vibrations of chelating and bridging bidentate carbonates, respectively, whereas the band at 1300−1325 cm^{-1} can be attributed to their overlapped sym ν_{O-C-O} modes. $\Delta\nu_3$ values of 325−355 and 425−445 cm^{-1} displayed by chelating and bridging bidentate carbonates, respectively, are in good agreement with the above proposed assignments. Finally, the band at 1050−1070 cm^{-1} should correspond to overlapping contributions of the three carbonate species.

Regarding the thermal stability of the adsorbed species, bridging bidentate carbonates are formed on the weakest basic sites, because they disappear above 323 K. Chelating bidentate and bicarbonates disappear above 373 and 473 K, respectively, whereas a fraction (between 9% for 2KUS723F and 30% for 1KUS723F) of unidentate carbonates remain even after evacuation at 673 K. In conclusion, unidentate carbonates correspond to the strongest sites determined in the calorimetric experiments, whereas bidentate and bicarbonate sites correspond to the weak sites or even the very weak sites not detected by calorimetry.

From the highest vibration modes of the spectra, a ratio between the strongest sites (unidentate carbonates) and weakest sites (bidentate carbonates and bicarbonates) can be obtained. On this basis, the decreasing order of basic sites strength is 1.4 (2KUS723F) > 1.1 (1KUS723F) > 0.7 (2K723F) > 0.4 (1K723F).

Therefore, there is a good correlation between this parameter and the reversibility/regenerability of the CO_2 adsorption. This result indicates that the strongest sites are correlated with unidentate modes of adsorption and are chiefly responsible for the irreversibility of the adsorption. These modes, however, have no positive effect on adsorption capacity, which is mainly controlled by the weakest adsorption sites. Both sonicated samples and samples prepared at high-supersaturation conditions tend to have higher concentrations of these sites, leading to highly irreversible adsorption.

4. Conclusions

The effects of several parameters (incorporated cation, mode of addition of magnesium and aluminum precursors, presence of sonication, and calcination temperature) on the prepara-
tion of magnesium−aluminum double oxides has been studied for CO_2 adsorption, including adsorbent regeneration. Thermogravimetric and calorimetric studies, as well as FTIR analysis, were used to understand the adsorption mechanisms leading to the undesirable irreversible adsorption.

Adsorption was conducted at both 323 and 373 K. A decrease in the uptake was observed as the adsorption temperature increased from 323 to 373 K, with the differences in adsorption capacity being caused by differences in both surface area and surface chemistry. Regarding the reversibility, sonication and high-supersaturation conditions in the preparation of the mixed oxides were found to lead to materials with the strongest basic sites. The presence of these sites was found to be related to the formation of unidentate CO_2-adsorbent species. The weaker basic sites, where bidentate and surface bicarbonates formed, were found to lead to highly reversible adsorption.

Acknowledgment

This work was supported by the Spanish Government (Contracts CTQ2008-06839-C03-02 and HF2007-0061). M.L. thanks the Government of the Principality of Asturias for a Ph.D. fellowship (Severo Ochoa Program).

Literature Cited

(1) Xu, X. C.; Song, C.; Andresen, J. M.; Miller, B. G.; Scaroni, A. W. Preparation and characterization of novel CO_2 "molecular basket" adsorbents based on polymer-modified mesoporous molecular sieve MCM-41. *Microporous Mesoporous Mater.* **2003**, *62*, 29–45.

(2) Przepiorski, M.; Skrodzewicz, M.; Morawski, A. W. High temperature ammonia treatment of activated carbon for enhancement of CO_2 adsorption. *Appl. Surf. Sci.* **2004**, *225*, 235–242.

(3) Inui, T.; Okugawa, Y.; Yasuda, M. Relationship between properties of various zeolites and their CO_2-adsorption behaviors in pressure swing adsorption operation. *Ind. Eng. Chem. Res.* **1988**, *27*, 1103–1109.

(4) Rege, S. U.; Yang, R. T.; Buzanowski, M. A. Sorbents for air prepurification in air separation. *Chem. Eng. Sci.* **2000**, *55*, 4827–4838.

(5) Delgado, J. A.; Uguina, M. A.; Sotelo, J. L.; Ruız, B. Fixed-bed adsorption of carbon dioxide−helium, nitrogen−helium and carbon dioxide−nitrogen mixtures onto silicalite pellets. *Sep. Purif. Technol.* **2006**, *49*, 91–100.

(6) Díaz, E.; Muñoz, E.; Vega, A.; Ordóñez, S. Enhancement of the CO_2 retention capacity of X zeolites by Na- and Cs-treatments. *Chemosphere* **2008**, *70*, 1375–1382.

(7) Díaz, E.; Muñoz, E.; Vega, A.; Ordóñez, S. Enhancement of the CO_2 retention capacity of Y zeolites by Na and Cs treatments: Effect of adsorption temperature and water treatment. *Ind. Eng. Chem. Res.* **2008**, *47*, 412–418.

(8) Choi, S.; Drese, J. H.; Jones, C. W. Adsorbent Materials for Carbon Dioxide Capture from Large Anthropogenic Point Sources. *ChemSusChem* **2009**, *2*, 796–854.

(9) Reddy, M. K. R.; Xu, Z. P.; Lu, G. Q.; da Costa, J. C. D. Influence of water on high-temperature CO_2 capture using layered double hydroxide derivatives. *Ind. Eng. Chem. Res.* **2008**, *47*, 2630–2635.

(10) Bellotto, M.; Rebours, B.; Clause, O.; Lynch, J.; Bazin, D.; Elkaim, E. Hydrotalcite decomposition mechanism: A clue to the structure and reactivity of spinel-like mixed oxides. *J. Phys. Chem.* **1996**, *100*, 8535–8542.

(11) Tichit, D.; Bennani, M. N.; Figueras, F.; Ruiz, J. R. Decomposition processes and characterization of the surface basicity of Cl^- and CO_3^{2-} hydrotalcites. *Langmuir* **1998**, *14*, 2086–2091.

(12) Corma, A.; Iborra, S. Optimization of alkaline earth metal oxide and hydroxide catalysts for base-catalyzed reactions. *Adv. Catal.* **2006**, *49*, 239–302.

(13) Climent, M. J.; Corma, A.; Iborra, S.; Epping, K.; Velty, A. Increasing the basicity and catalytic activity of hydrotalcites by different synthesis procedures. *J. Catal.* **2004**, *225*, 316–326.

(14) Abelló, S.; Medina, F.; Tichit, D.; Pérez-Ramírez, J.; Rodríguez, X.; Sueiras, J. E.; Salagre, P.; Cesteros, Y. Study of alkaline-doping agents on the performance of reconstructed Mg−Al hydrotalcites in aldol condensations. *Appl. Catal. A* **2005**, *281*, 191–198.

(15) Sharma, S. K.; Kushwaha, P. K.; Srivastava, V. K.; Bhatt, S. D.; Jasra, R. V. Effect of hydrothermal conditions on structural and textural properties of synthetic hydrotalcites of varying Mg/Al ratio. *Ind. Eng. Chem. Res.* **2007**, *46*, 4856–4865.

(16) Reddy, M. K. R.; Xu, Z. P.; Lu, G. Q.; da Costa, J. C. D. Layered double hydroxides for CO_2 capture: Structure evolution and regeneration. *Ind. Eng. Chem. Res.* **2006**, *45*, 7504–7509.

(17) Prescott, H. A.; Li, Z.; Kemnitz, E.; Trunschke, A.; Deutsch, J.; Lieske, H.; Auroux, A. Application of calcined Mg−Al hydrotalcites for Michael additions: An investigation of catalytic activity and acid−base properties. *J. Catal.* **2005**, *234*, 119–130.

(18) Duan, X.; Evans, D. G. *Layered Double Hydroxides*; Springer: Berlin, 2006.

(19) Wang, X. P.; Yu, J. J.; Cheng, J.; Hao, Z. P.; Xu, Z. P. High-temperature adsorption of carbon dioxide on mixed oxides derived from hydrotalcite-like compounds. *Environ. Sci. Technol.* **2008**, *42*, 614–618.

(20) Ficicilar, B.; Dogu, T. Breakthrough analysis for CO_2 removal by activated hydrotalcite and soda ash. *Catal. Today* **2006**, *115*, 274–278.

(21) Yang, W.; Kim, Y.; Liu, P. K. T.; Sahimi, M.; Tsotsis, T. T. A study by in situ techniques of the thermal evolution of the structure of a Mg−Al−CO_3 layered double hydroxide. *Chem. Eng. Sci.* **2002**, *57*, 2945–2953.

(22) Hutson, N. D. Structural effects on the high temperature adsorption of CO_2 on a synthetic hydrotalcite. *Chem. Mater.* **2004**, *16*, 4135−4143.

(23) Othman, M. R.; Rasid, N. M.; Fernando, W. J. N. Mg−Al hydrotalcite coating on zeolites for improved carbon dioxide adsorption. *Chem. Eng. Sci.* **2006**, *61*, 1555–1560.

(24) Rives, V. *Layered Double Hydroxide: Present and Future*; Nova Science Publishers: New York, 2001.

(25) Hickey, L.; Kloprogge, J. T.; Frost, R. L. The effects of various hydrothermal treatments on magnesium−aluminium hydrotalcites. *J. Mater. Sci.* **2000**, *35*, 4347–4355.

(26) Carriazo, D.; del Arco, M.; Martín, C.; Rives, V. A comparative study between chloride and calcined carbonate hydrotalcites as adsorbents for Cr(VI). *Appl. Clay Sci.* **2007**, *37*, 231–239.

(27) Jenkins, R.; Snyder, R. L. *Introduction to X-ray Powder Diffractometry*; John Wiley & Sons: New York, 1996.

(28) Yu, J. J.; Jiang, Z.; Zhu, L.; Hao, Z. P.; Xu, Z. P. Adsorption/desorption studies of NO_x on well-mixed oxides derived from Co−Mg/Al hydrotalcite-like compounds. *J. Phys. Chem. B* **2006**, *110*, 4291−4300.

(29) Meloni, D.; Monaci, R.; Solinas, V.; Auroux, A.; Dumitriu, E. Characterisation of the active sites in mixed oxides derived from LDH precursors by physico-chemical and catalytic techniques. *Appl. Catal. A* **2008**, *350*, 86–95.

(30) Ebner, A. D.; Reynolds, S. P.; Ritter, J. A. Understanding the adsorption and desorption behavior of CO_2 on a K-promoted hydrotalcite-like compound (HTlc) through nonequilibrium dynamic isotherms. *Ind. Eng. Chem. Res.* **2006**, *45*, 6387–6392.

(31) Ebner, A. D.; Reynolds, S. P.; Ritter, J. A. Nonequilibrium kinetic model that describes the reversible adsorption and desorption behavior of CO_2 in a K-promoted hydrotalcite-like compound. *Ind. Eng. Chem. Res.* **2007**, *46*, 1737–1744.

(32) Auroux, A. Acidity characterization by microcalorimetry and relationship with reactivity. *Top. Catal.* **1997**, *4*, 71–89.

(33) Atkins, P. W. *Physical Chemistry*, 6th ed.; Oxford University Press: Oxford, U.K., 2000.

(34) Auroux, A.; Monaci, R.; Rombi, E.; Solinas, V.; Sorrentino, A.; Santacesaria, E. Acid sites investigation of simple and mixed oxides by TPD and microcalorimetric techniques. *Thermochim. Acta* **2001**, *379*, 227–231.

(35) Prinetto, F.; Ghiotti, G.; Durand, R.; Tichit, D. Investigation of acid−base properties of catalysts obtained from layered double hydroxides. *J. Phys. Chem. B* **2000**, *104*, 11117–11126.

(36) Lavalley, J. C. Infrared spectrometric studies of the surface basicity of metal oxides and zeolites using adsorbed probe molecules. *Catal. Today* **1996**, *27*, 377–401.

(37) Ramis, G.; Busca, G.; Lorenzelli, V. Low-temperature CO_2 adsorption on metal oxides: Spectroscopic characterization of some weakly adsorbed species. *Mater. Chem. Phys.* **1991**, *29*, 425–435.

Received for review December 30, 2009
Revised manuscript received February 17, 2010
Accepted February 22, 2010

IE902072A